LA-UR- 04-0649

Approved for public release; distribution is unlimited.

Title: Structure and Property Evolutions of Ecaped 7075 AL Alloy During Annealing

Author(s): Yonghao Zhao, Xiaozhou Liao, Yuntian Zhu, R. Z. Valiev

Submitted to: 2004 TMS Conference Proceeding
Charlotte, NC
March 14-18, 2004

Los Alamos
NATIONAL LABORATORY

Ultrafine Grained Materials III *Edited by Y.T. Zhu, T.G. Langdon, R.Z. Valiev, S.L. Semiatin, D.H. Shin, and T.C. Lowe.* **TMS (The Minerals, Metals & Materials Society), 2004**

STRUCTURE AND PROPERTY EVOLUTIONS OF ECAPED 7075 AL ALLOY DURING ANNEALING

Y.H. Zhao[1], X.Z. Liao[1], Y.T. Zhu[1*], and R.Z. Valiev[2]

[1]Materials Science and Technology Division, Los Alamos National Laboratory
Los Alamos, NM 87545
[2]Institute of Physics of Advanced Materials, Ufa State Aviation Technical University
12 K. Marx Street, 450000 Ufa, Russian Federation

Abstract

Structure and microhardness evolutions of equal-channel angular pressing (ECAP) processed and coarse-grained (CG) 7075 Al alloys during differential scanning calorimeter (DSC) were investigated by x-ray diffraction (XRD), transmission electron microscopy (TEM) and microhardness measurements. After one-month aging at room temperature, the microhardness of the ECAP processed sample is about 50% larger than that of the CG sample. During DSC annealing, the microhardness of the ECAP processed sample decreased gradually, while a hardening peak appeared for the CG sample. XRD and TEM show that the hardening peak of the CG sample was mainly caused by the precipitation hardening of the Guinier-Preston (GP) zone. For the ECAP processed sample, upon annealing the microstrain (dislocation density) decreased and the crystallites grew, which decreased the hardness and overcompensated the GP zone precipitation hardening. DSC analysis indicates ECAP process only promoted the phase precipitation, but did not change the sequence of phase precipitation.

Keywords: severe plastic deformation, Al alloy, aging hardening, microhardness, grain size, microstrain, lattice parameter, dislocation density.

Introduction

In the last decade, considerable efforts have been devoted to the fabrication of ultrafine grained (UFG) materials (with grain size in submicrometer or nanometer range) by severe plastic deformation (SPD) methods. As a result, several techniques, such as equal channel angular pressing (ECAP) [1] and high-pressure torsion (HPT) [2] were developed to successfully introduce UFG structures into various pure metals and alloys. Of these techniques, ECAP is especially attractive because it can produce relatively large bulk UFG samples without changing the cross-sectional dimensions of the sample. During an ECAP process, the sample was deformed by being pressed through a die containing two channels, equal in cross section and intersecting at a certain angle. Consecutive pressings were conducted to attain a high total strain. The bulk UFG materials are thought to have considerable potential industrial applications due to their high strength with good ductility and superplasticity at moderate temperatures and high strain rates, etc. [3].

A significant amount of work has been reported on ECAP processing Al-Mg alloy which is well known as a work hardening alloy [4-6]. However, much less attention has been paid to the precipitate hardening Al-Zn-Mg 7000 series alloys, which show the highest strength of all commercial Al alloys and are widely used for structural applications in military and civil aircrafts. ECAP process introduces a large amount of defects (such as dislocation and grain boundary) into the alloy. These defects may affect the phase precipitations, and change the mechanical properties. The 7000 Al alloys are strengthened by precipitation hardening during the aging of the supersaturated solid solution. The precipitation sequence is [7-10]:

Supersaturated solid solution $\rightarrow$ Guinier-Preston (GP) zone $\rightarrow$ $\eta'(MgZn_2) \rightarrow \eta(MgZn_2)$

*Corresponding author. yzhu@lanl.gov

The GP zone is coherent with the matrix and have a spherical shape. The interfacial energy for GP zone in Al-Zn-Mg-Cu 7075 system is so low that a high density of very small-size zones (≤ 7.5 nm) can be formed at room temperature. The semicoherent intermediate metastable phase η′ (10 to 30 nm) and the incoherent equilibrium phase η (40 to 80 nm) have hexagonal structures. But the lattice constant of η′ is a little larger than that of η. The high strength of 7075 is found to be associated with a high density of GP zones, which increase the resistance to dislocation movement arising from the strong atomic bonds in the zones.

The objective of this work was to investigate the microstructure (phase precipitation, grain size, microstrain, lattice parameter and dislocation density) and property (microhardness) characteristics of 7075 Al alloy processed by ECAP following one-month natural aging at room temperature, and their evolutions during nonisothermal annealing (with a constant heating rate). For the purpose of comparison, coarse-grained (CG) 7075 sample subjected to the same natural aging was also characterized.

Experimental Procedures

Commercial 7075 Al alloy was homogenized by solution treatment for 5 h at 480 °C and quenched to room temperature. The initial grain size is approximately 40 μm. An ECAP die with an intersecting channel angle of 90° and an outerarc angle of 45° was used. Sample was processed for 2 passes by route B_c in which the work piece was rotated 90° along its longitudinal axis between adjacent passes. The ECAP processed UFG and initial CG samples were naturally aged at room temperature for one month, then were cut into small pieces in an orientation perpendicular to the pressing direction. These thin pieces were polished from each side to remove the surface layer. Disks with a diameter of approximately 5 mm were then cut from the polished samples for the following characterizations.

Thermal analysis was performed in a Perkin-Elmer differential scanning calorimeter (DSC-7). The polished alloy disks (approximately 30 mg) were sealed in Al pans and heated in a flowing Ar atmosphere at constant heating rates of 5 and 10 °C/min, respectively. Two DSC-runs were successively performed on each sample; the second run was used to obtain the baseline. To measure the property and microstructure evolution during annealing, the samples were linearly heated to the exothermic and endothermic peak temperatures and post peak temperatures, then were quenched to room temperature at a cooling rate of 400 K/min.

Microhardness measurements were carried out on Buehler Micromet® Hardness Tester with a load of 500 g and loading time of 15 s. The indenter is the Vickers diamond pyramid. For each sample, at least 20 points were measured to get an average value with a typical uncertainty of ±2 %. The quantitative x-ray diffraction (XRD) measurements were performed on a Scintag x-ray diffractometer, which was equipped with a Cu target operating at 1.8 kW and a secondary monochromator to select the Cu K_α radiation. θ-2θ scan with a step size of $2\theta = 0.02°$ and a counting time of 10 s was performed at room temperature. Pure Al powder (99.999%) was annealed at 200 °C in Ar and used as XRD reference. Transmission electron microcopy (TEM) was performed using a Phillips CM30 microscope operated at 300 kV. The TEM sample was prepared by mechanical grinding of the annealed 7075 Al alloys disks to a thickness of about 10 μm. Further thinning to a thickness of electron transparency was carried out using a Gatan Precision Ion Milling System with an Ar+ accelerating voltage of 4 kV.

Results and Discussion

Thermal Analysis and Microhardness

Figures 1(a) shows the DSC scans for the ECAP processed UFG and initial CG samples with heating rates of 5 and 10 °C/min, respectively. Both samples have two endothermic peaks at about 100 °C and 250 °C, respectively, and two overlapped exothermic peaks at about 200 °C. With increasing heating rate, all the peaks moved towards higher temperatures. Comparison with previous results indicates that the low temperature endotherm (Region I) is due to GP zone dissolution, the high temperature endotherm (Region III) is due to η dissolution, and the intermediate region (Region II) consists of two overlapped exotherms (IIA and IIB) including GP zone and η′ formations, and η formation [11,12]. However, there are some differences in the DSC curves between the two samples. The first endotherm of the CG sample is broader and the peak temperature is lower than that of the UFG sample. The two exothermic peaks of the

CG sample overlapped much more than those of the UFG sample. In addition, the first exotherm peak position of the UFG sample is much lower than that of the CG sample, which suggests that large amount of defects in the UFG sample promote GP zone and η′ precipitation. The second endotherm of the UFG sample is much broader than that of CG sample.

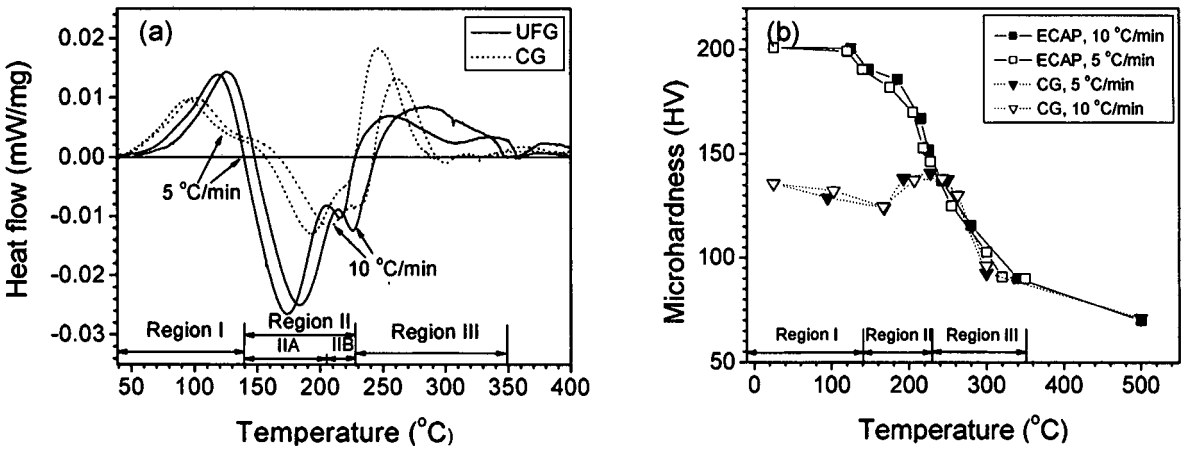

Figure 1. DSC scans (a) and microhardness (b) of the UFG and CG samples (heating rate: 5, 10 °C/min).

By integrating the area of the peak, we obtained the enthalpies of the different reactions, *ΔH*, as listed in Table 1. For the first endotherm, the enthalpy of the UFG sample is equivalent to that of the CG sample. For the exotherms and the second endotherm, the enthalpies of the UFG sample are evidently larger than those of the CG sample.

Table 1. The enthalpies of the different reactions during DSC annealing for the UFG and CG samples.

ΔH (J/g)	Region I	Region II	Region III
UFG	7.04	-14.27	6.99
CG	6.98	-8.48	4.29

The microhardness evolutions against DSC annealing with heating rates of 5 and 10 °C/min was shown in Fig. 1(b). For the UFG sample, the microhardness decreased gradually upon annealing. While for the CG sample, the microhardness decreased at region I, increased at region II, then decreased at region III. That is, the CG sample has a hardening peak in region II and III. In region III, the microhardness of the UFG and CG samples have the same decreasing tendency. The microhardness of initial UFG sample is about 50% larger than that of CG sample.

Phase Precipitation

The XRD results of the UFG and CG samples at different DSC annealing temperatures with a heating rate of 5 °C/min were shown in Figs. 2(a,b). The diffraction planes of the hexagonal η were also indicated in the figures. Both UFG and CG samples have the similar variations against DSC annealing. For the initial UFG and CG samples, besides the Al Bragg reflections, there is a broad peak at about 20° and other weak peaks whose positions are a little lower than those of η phase. These weak peaks correspond to hexagonal η′, whose lattice parameters are reported to be a little larger than those of η [7]. During annealing in region I (GP zone dissolution), the broad peak at about 20° was weakened significantly, indicating this broad peak corresponds to GP zone; while the peaks of η′ have no evident variation. Because the XRD sample has the same area involved in the reflection, the intensity of the XRD patterns can be compared. In region IIA, the GP zone was formed again and grew into η′ phase (see the variation of the broad peak at about 20°). At the end of region IIA, the intensities of η′ peaks (between Al(111) and (200) peaks) increased significantly, suggesting a large amount of η′ precipitation. In region IIB, the η′ peaks gradually moved towards those of η, indicating that part of η′ gradually grew into η. At the end of region IIB, the little lower deviation of the peaks to those of η indicates there exists a mixture of η′ and η phases. In region III, the peaks turned

sharper and moved to η position, suggesting all η′ transformed into η and η particles coarsened.

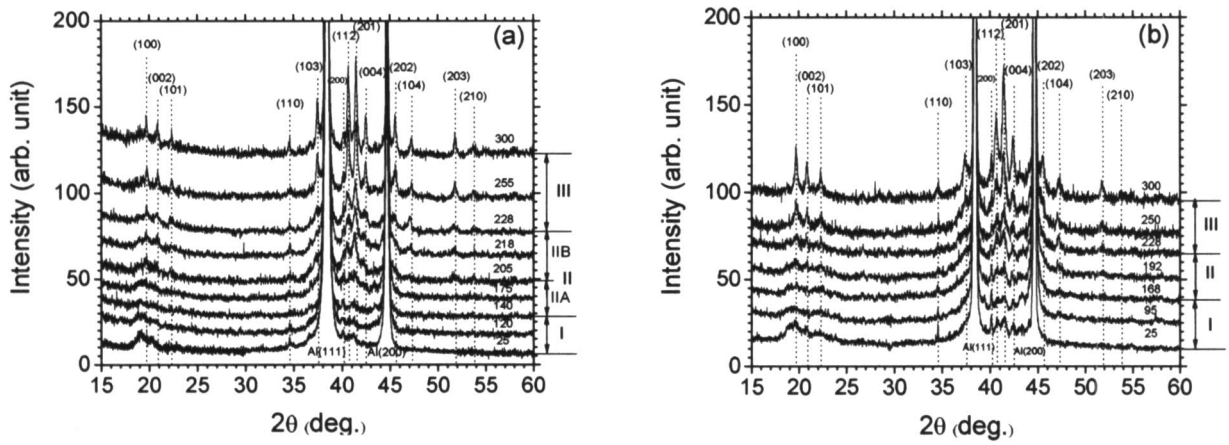

Figure 2. XRD results of the UFG (a) and CG (b) samples annealed at different temperatures by DSC.

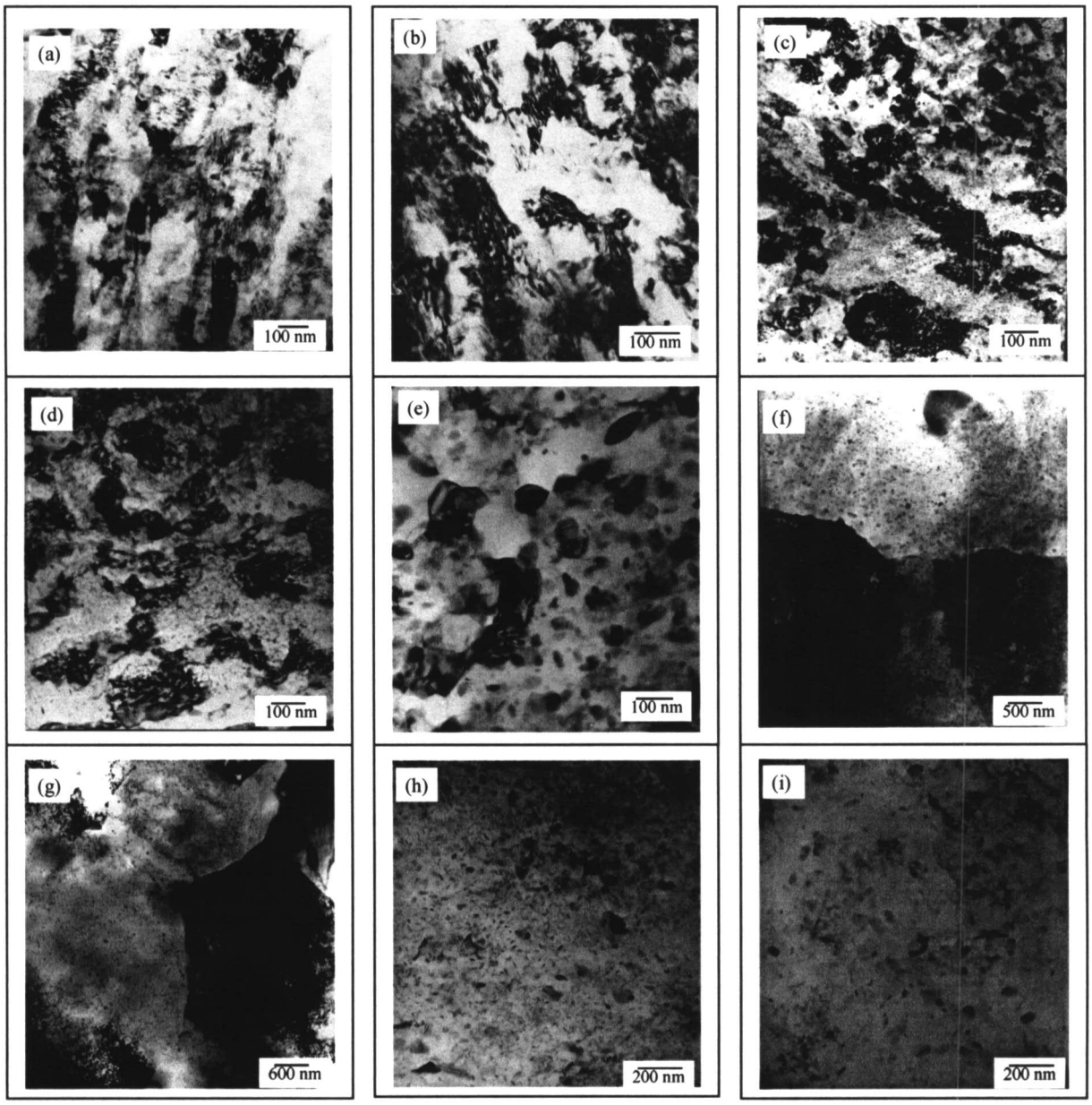

Figure 3. TEM pictures of UFG (a-e) and CG (f-i) samples annealed at a heating rate of 5 °C/min (a) 25 °C, (b) 140 °C, (c) 205 °C, (d) 228 °C (e) 300 °C; (f) 25 °C, (g) 168° C (h) 228 °C, (i) 300 °C.

The above phase precipitation can be observed by TEM, as shown in Figs. 3 (a-i). For the initial natural aged ECAP and CG samples, spherical GP zones (with diameter smaller than 7.5 nm) and plate-shaped η′ (10-30 nm) are observed (Figs 3a and 3f). This indicates that a large amount of GP zone and a small amount of η′ were formed during the one-month room-temperature aging. After the fist endotherm (Figs. 3b and 3g), the amount of GP zone was reduced significantly, caused by the dissolution of GP zone. At the end of the first exotherm (region IIA), large amount of spherical GP zone and plate-shaped η′ phase precipitated out (see Fig. 3c). After the second exotherm (region IIB), there appeared large amount of needle-shaped phase (40-80 nm) mixed with plate-shaped η′ (Figs. 3d and 3h). The needle-shaped phase was verified to be hexagonal η phase [9, 10]. At the end of region III, only η needles and coarsened η particles (larger than 100 nm) were observed (Figs. 3e and 3i).

Microstructural Evolution

The grain size and microstrain of the UFG sample can be calculated from XRD broadening peaks by Scherrer and Wilson method [13], as shown in Figs. 4(a,b). From TEM pictures, one can get the grain size statistic distribution and the average grain size, see Fig. 4(a).

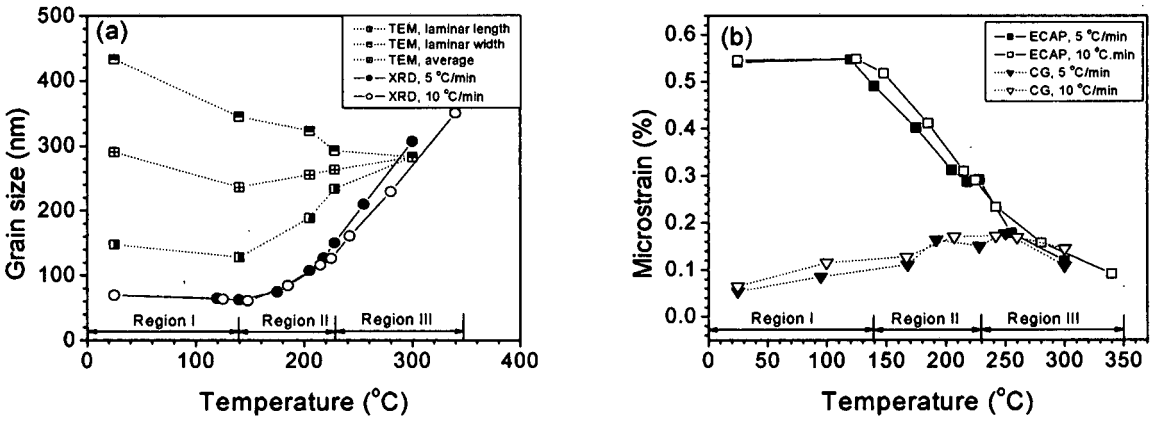

Figure 4. Grain size (a) and microstrain (b) of UFG and CG samples calculated from XRD and TEM.

For the initial ECAP sample (Fig. 3a), TEM showed lamella grains with a length of about 430 nm and a width of about 150 nm, which was produced by the shear deformation during ECAP process. During DSC annealing the lamella length decreased and the lamella width increased due to recovery and recrystallization. As a result, the mean grain size averaged from the lamella grain length and width did not change much during DSC annealing. From Figs. 3(c) and 3(d), evident recovery and recrystalization occurred when the UFG sample was annealed to 205 and 228 °C. Recystallization completed when the temperature reached 300 °C (Fig. 3e). The grain size calculated from XRD results are smaller than those from TEM, this is because XRD calculated the subgrain size even if they have very small orientation difference. From XRD results, the grain size of the UFG sample increased from about 70 nm to 310 nm during the DSC annealing. The grain growth of the sample annealed by 10 °C/min is less than that of the sample annealed by 5 °C/min. From TEM, the grain size of the CG sample increased from about 40 μm to 50 μm during annealing. From Fig. 4(b), the microstrain of the UFG sample decreased significantly from about 0.5 % to 0.1 % in region II and III. While the microstrain of the CG sample increased slightly from 0.05 % to 0.15 % during DSC annealing.

Figure 5(a) shows the lattice parameter evolutions of the UFG and CG Al alloys during DSC annealing, which was calculated from the XRD peak positions. The lattice parameters of both UFG and CG samples have similar changes: increased from 4.056 Å to about 4.059 Å in region I, and decreased significantly in region II, then increased slightly in region III. These can be explained by GP zone dissolution in region I, GP zone, η′ and η precipitation in region II, and η dissolution in region III. The dissolution of atoms of Mg and Zn etc. into Al matrix will increase the Al lattice constant, the reverse process will decrease Al lattice constant.

The dislocation density in the UFG and CG samples can be calculated from the grain size and microstrain [14,15], as shown in Fig. 5(b). The dislocation density of the UFG sample

decreased from about $1.0\times10^{14}m^{-2}$ to about zero in region II and III. For the CG sample, the dislocation density is remained at ~0 during annealing

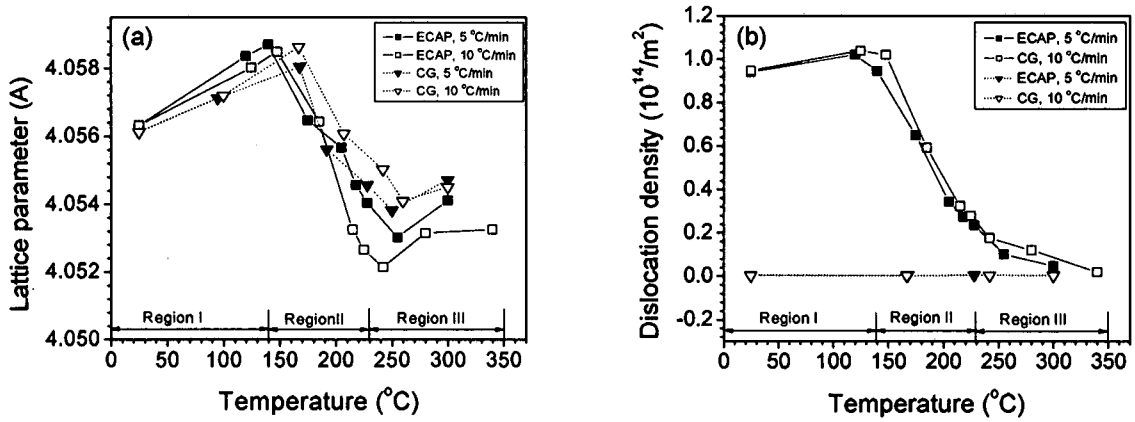

Figure 5. Lattice parameter (a) and dislocation density (b) of the UFG and CG samples (5, 10 °C/min).

The current experiments show that the ECAP processed 7075 Al alloy has much higher hardness than the CG sample. The UFG 7075 Al alloy have (i) solid solution strengthening, (ii) grain refinement strengthening, (iii) dislocation strengthening and (iv) precipitation strengthening. The first two effects appear to have less contributions compared to the last two effects. Because in region III the UFG and CG samples have the same microhardness even though their grain sizes are very different. The hardening peak of the CG sample in region II is caused by GP zone formation, while for the UFG sample, the hardening peak in region II disappeared because the dislocation density decreased largely in region II and overcompensated the GP zone hardening. The recovery of large amount of defects in region II can also have contribution to the large exothermic enthalpy of the UFG sample.

Conclusion

The microhardness of the ECAP processed 7075 Al alloy is about 50 % larger than that of the CG sample. During DSC linear-heating annealing, there exists a hardening peak for the CG sample caused by GP zone formation, while for the UFG sample, the hardening peak was overcompensated by the significantly decreased dislocation density. DSC indicates ECAP process only promoted phase precipitation, did not change the phase precipitation sequence.

Reference

1. V.M. Segal, V.I. Reznikov, A.E. Drobyshevskiy and V.I. Kopylov, Russ. Metall. (Metally), 1 (1981), 99-105.
2. H. Jiang, Y.T. Zhu, D.P. Butt, I.V. Alexandrov, T.C. Lowe, Mater. Sci. Eng., A290 (2000), 128-138.
3. R.Z. Valiev, R.K. Islamgaliev and I.V. Alexandrov, Prog. Mater. Sci., 45 (2000), 103-189.
4. Y. Iwahashi, Z. Horita, M. Nemoto and T.G. Langdon, Acta Mater. 45 (1997), 4733-4741.
5. M. Furukawa, A. Utsunomiya, K. Matsubara, Z. Horita, T.G. Langdon, Acta Mater. 49 (2001), 3829-3838.
6. S. Lee, A. Utsunomiya, H. Akamatsu, K. Neishi, M. Furukawa, Z. Horita and T.G. Langdon, Acta Mater. 50 (2002), 553-564.
7. L.F. Mondolfo, N.A. Gjostein and D.W. Levinson, Tans. Amer. Inst. Min. (Metall.) Engrs., 206 (1956), 1378-1392.
8. H. Schmalzried, H. Gerold, Z. Metallkd., 49 (1958), 291-301.
9. G. Thomas and J. Nutting, J. Inst. Met., 88 (1959-60), 81-90.
10. J.D. Embury and R.B. Nicholson, Acta Metall., 13 (1965), 403-417.
11. P.N. Adler and R. Delasi, Metall. Trans. A, 8A (1977), 1185-1190.
12. J.M. Papazian, Metall. Trans. A, 13A (1982), 761-769.
13. Y.H. Zhao, K. Zhang and K. Lu, Phys. Rev. B, 56 (1997), 14322-14330.
14. Y.H. Zhao, H.W. Sheng and K. Lu, Acta Mater. 49 (2001), 365-375.
15. Y.H. Zhao, K. Zhang and K. Lu, Phys. Rev. B, 66 (2002), 085404-01—08.